

# HRTEM study of [001] low-angle tilt grain boundaries in fiber-textured BaTiO<sub>3</sub> thin films

M. Igarashi · Y. Sato · N. Shibata · T. Yamamoto ·  
Y. Ikuhara

Received: 17 November 2005 / Accepted: 15 February 2006 / Published online: 27 July 2006  
© Springer Science+Business Media, LLC 2006

**Abstract** Low-angle tilt grain boundaries in [001] fiber-textured BaTiO<sub>3</sub> thin films were investigated by high-resolution transmission electron microscopy. Extensive observation revealed a very high density of low-angle tilt grain boundaries in the film. The low-angle tilt grain boundaries can be described as periodical arrays of dislocations on {100} and {110} boundary planes. The boundaries with (100) plane on {100} planes are composed of perfect dislocations with Burgers vectors  $\mathbf{b} = a < 100 >$  ( $a$  = lattice constant of BaTiO<sub>3</sub>: 0.3992 nm), while the boundaries with (110) plane on {110} planes are composed of the dissociated dislocations with Burgers vectors  $a/2 < 110 >$ . It was thus found that the difference in the boundary plane leads to different dislocation structures along the low-angle grain boundaries.

## Introduction

Functional properties of oxide ceramics often originate from the presence of grain boundaries. Electroceramics, such as BaTiO<sub>3</sub>, are typical examples, and showing a positive temperature coefficient of resistivity (PTCR) [1]. The electrostatic potential barrier formed at grain

boundaries is thought as the origin of the PTCR effect in BaTiO<sub>3</sub> [2]. Thus, it is important to understand the mechanism of barrier formation at grain boundaries in electroceramic materials.

It is reported that the PTCR of BaTiO<sub>3</sub> single boundaries strongly depends on the orientation of grain boundaries. Coherent boundaries, such as low-angle and coincidence-site-lattice [3] (CSL) boundaries showed smaller PTCR, whereas incoherent boundaries exhibited larger ones [4, 5]. This indicates that an understanding for the atomic structures of BaTiO<sub>3</sub> boundaries is important to clarify the mechanism of the potential barrier formation.

In this study, BaTiO<sub>3</sub> films with a [001] fiber-texture were fabricated by pulsed laser deposition (PLD), in order to investigate atomic structures of many types of grain boundaries. As will be noted later, the fiber is normal to the substrate plane and the grain boundaries are normal to the substrate plane to minimize the boundary energy. Thus, mostly [001] tilt grain boundaries exist in the films, which is very suitable for high-resolution transmission electron microscopy (HRTEM) observations. Here, we focus on the atomic structure of low-angle tilt boundaries, which were frequently found in the films and thus one of the stable grain boundary structures in this material.

## Experimental Procedure

In the present study, BaTiO<sub>3</sub> was deposited on [0001] fiber-textured ZnO films [6] grown on quartz-grass substrates. First, ZnO was deposited on quartz-grass substrates at a substrate temperature of 400 °C and then BaTiO<sub>3</sub> films were deposited at the elevated

M. Igarashi · Y. Sato · T. Yamamoto  
Department of Advanced Materials Science, The University of Tokyo, 5-1-5 Kashiwanoha, Kashiwa, Chiba 277-8651, Japan

N. Shibata · Y. Ikuhara (✉)  
Institute of Engineering Innovation, The University of Tokyo, 2-11-16 Yayoi, Bunkyo-ku, Tokyo 113-8656, Japan  
e-mail: ikuhara@sigma.t.u-tokyo.ac.jp

temperature of 750 °C. For both films, a KrF excimer laser beam (wavelength: 248 nm; repetition frequency: 10 Hz) was used for the deposition. During the deposition, an oxygen partial pressure and a backpressure were kept at a constant value of  $1.0 \times 10^{-3}$  Pa and  $1.3 \times 10^{-5}$  Pa, respectively. The obtained films were annealed at 800 °C for 3 h in air to obtain energetically favorable grain boundaries. X-ray diffractometry revealed that the BaTiO<sub>3</sub> film has a sharp [001] fiber-texture structure, probably induced by the templating [0001] fiber-textured ZnO films.

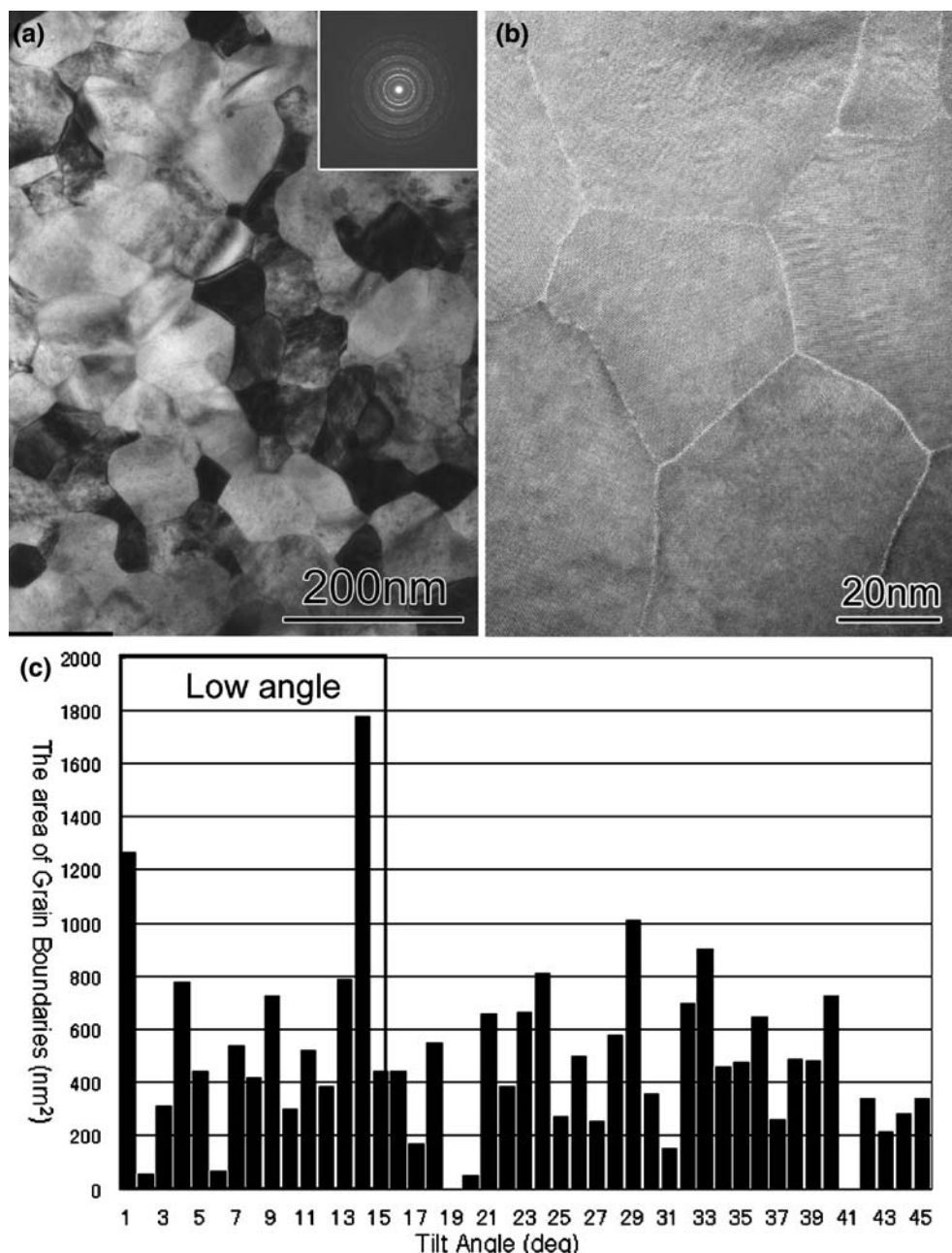
Plan-view TEM thin foils were prepared by ion beam thinning only from the substrate side (Duomill Model

600 with ion energies of 3–4 keV and a beam angle of 17°, Gatan, Inc., Pleasanton, CA) to obtain an electron transparency. Transmission electron microscopy (TEM) observation was conducted by using a JEM-2010 HC and a JEM-4010 (JEOL Co. Ltd., Japan) transmission electron microscope with an accelerating voltage of 200 kV and 400 kV, respectively.

## Results and Discussion

Figure 1(a) shows a bright-field TEM image of a BaTiO<sub>3</sub> film with an average grain size of less than

**Fig. 1** (a) Bright-field TEM image of BaTiO<sub>3</sub> films. The inset shows a selected area diffraction pattern. (b) HRTEM image of the film observed from [001] direction. (c) A histogram showing the relationship between tilt angle and the area of the boundaries



50 nm. The inset shows a selected-area diffraction pattern (SADP) obtained from the BaTiO<sub>3</sub> film. The ring-like intensity patterns clearly indicate a formation of polycrystalline BaTiO<sub>3</sub>, but it was also found that only the spots from (hkl) ( $l = 0$ ) planes are present in this pattern, indicating that all the grains have common [001] axes parallel to the incident beam direction. Fig. 1(b) shows a HRTEM image of the BaTiO<sub>3</sub> film. Since all grains have common [001] axes, all the boundaries are [001] tilt-type grain boundaries and, therefore, the atomic structures can be observed for all the boundaries.

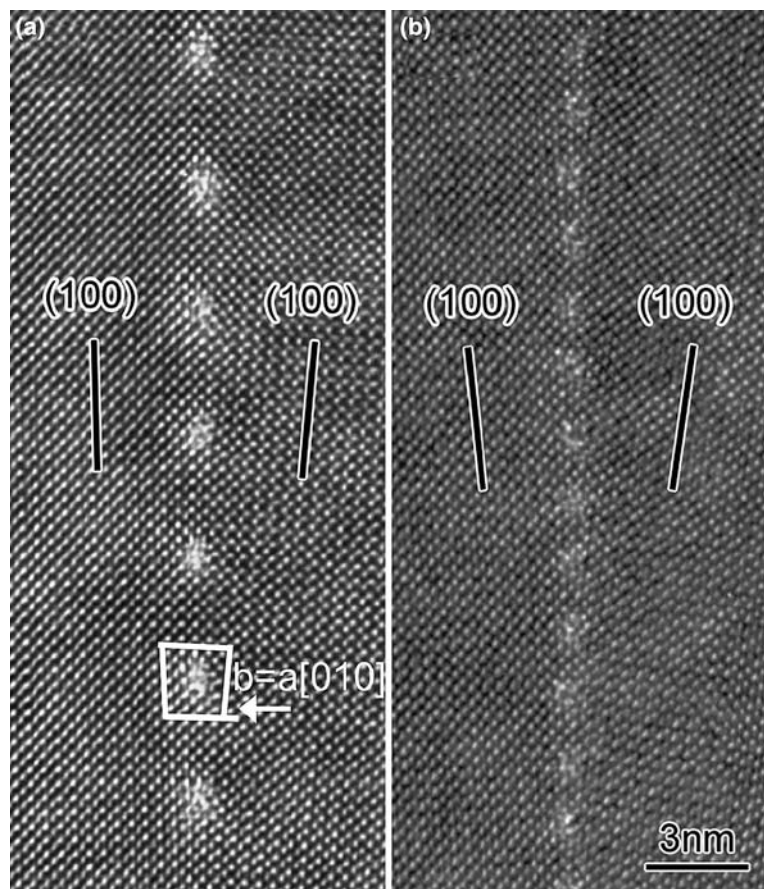
HRTEM observations were conducted for a number of boundaries in the BaTiO<sub>3</sub> film. Fig. 1(c) shows a plot of tilt angle against sum of the area of 118 grain boundaries. Here, the boundary area was calculated by multiplying the projected length and the sample thickness. The projected length was directly measured from the images and the sample thickness was assumed to be 5 nm for all the boundaries. It is found that low-angle grain boundaries with a tilt angle of 0°~15° (over 40%) are frequently found in the film. This indicates that low-angle grain boundaries are one of the stable, common grain boundaries in BaTiO<sub>3</sub> materials. It is

also interesting to point out that the low-angle grain boundaries can be classified into two groups; one with (100) boundary planes, and the other with (110) boundary planes. No other boundary planes were observed in this study, and some of the boundaries are composed of the combination of two boundary planes, which will be shown later.

Figure 2 shows HRTEM images of (a) 7.6° and (b) 12.6° tilt grain boundaries with the grain boundary plane of (100). Periodical arrays of strong contrast, which is associated with edge dislocations, are recognized in these images. In Fig. 2(a), a Burgers circuit is drawn to include one dislocation. The Burgers vector of the dislocation is found to be  $\mathbf{b} = a[100]$ , which is the perfect type dislocation. All dislocations in Fig. 2(a) and (b) have the same type of Burgers vector. The distance between neighboring dislocations is estimated to be about 3.0 nm from (a) and 1.8 nm from (b). This is consistent with the predicted value (3.0 nm and 1.8 nm) from the Frank's equation [7] estimating the dislocation periodicity by simple geometric considerations.

On the other hand, low-angle boundaries with a boundary plane of (110) exhibit different features, as

**Fig. 2** HRTEM images of the [001] tilt grain boundaries on (100) plane with the misorientation angle of (a) 7.6° and (b) 12.6°



shown in Fig. 3(a) and (b). Fig. 3(a) and (b) shows HRTEM images of (a) 4.0° and (b) 10.0° tilt boundaries with the boundary plane of (110). An array of edge dislocations was also observed in these images. However, it was found that each perfect dislocation is dissociated into two partials ( $a [110] \rightarrow a/2 [110] + a/2 [\bar{1}10]$ ).

In Fig. 3(a) and (b), the distance between two partial dislocations, that is, the length of stacking fault, is estimated to be about 1.1–1.4 nm. This is a slightly shorter value than (2.2–2.8 nm [8] or 1.8–2.5 nm [9]) observed in  $\text{SrTiO}_3$ .

Figure 4(a) and (b) show schematics of the edge dislocations in low-angle grain boundaries with the boundary plane of (a) (100) and (b) (110). As shown in (a), ions with like signs become too close to each other at the stacking fault region in the case of (100) boundary. Since this should result in a rather high stacking fault energy, this seems to be the reason why (100) low-angle boundary cannot dissociate into two partials. On the other hand, such an energetically unfavorable configuration seems not to occur in the (110) boundary. Ions with like signs do not become too close at the region of stacking fault in this dislocation,

because the stacking sequence of (110) plane with alternating cation and anion planes is not disturbed even by the formation of the stacking fault. This would result in a relatively lower stacking fault energy than in the case of the (100) stacking fault. Thus, a decomposition of from a perfect dislocation ( $a [110]$ ) into two partials ( $a/2 [110] \times 2$ ) with a stacking fault can be possible on the present boundary plane.

Through the observations of a number of low-angle boundaries, all the dislocations in low-angle boundaries observed in the  $\text{BaTiO}_3$  film can be classified into these two types, that is, (100) and (110) types, as also the case in  $\text{YBa}_2\text{Cu}_3\text{O}_{7-\delta}$  [10].

A typical example of a curved low-angle grain boundary is shown in Fig. 5. Here, we only find segments of (100) and (110) boundary planes. In the region with the boundary plane of (100), a periodical array of the perfect dislocations of  $a [100]$  is observed. On the other hand, the boundary plane of (110) is found in the curved regions, and dissociated dislocations of  $a/2 [110] + a/2 [\bar{1}10]$ , which are indicated by the arrows, are also found in these regions. We conclude that these two dislocation structures must be the stable structure of [001] low-angle tilt grain boundaries in  $\text{BaTiO}_3$ .

**Fig. 3** HRTEM images of the [001] tilt grain boundaries on (110) plane with the misorientation angle of (a) 4.0° and (b) 10.0°

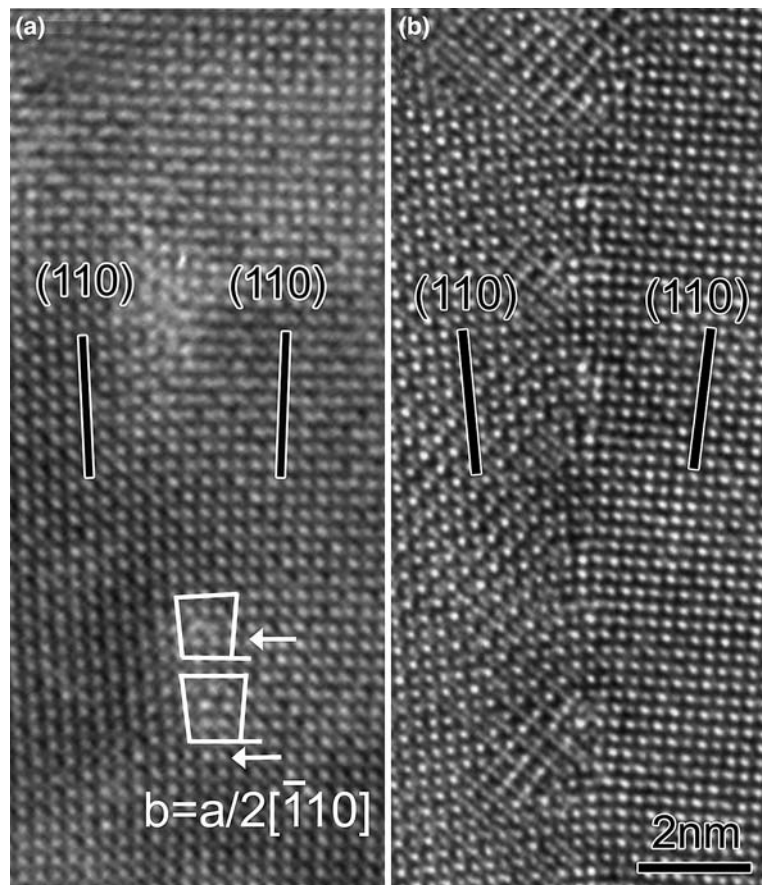


**Fig. 4** Schematics showing the structure of the (a) [001] tilt boundary on (100) plane with dissociated partial dislocations and a stacking fault and (b) [001] tilt boundary on (110) plane with dissociated partial dislocations and stacking fault. The positions of partial dislocations are indicated by the reversed “T” shapes and the ellipses show the regions including stacking faults. Small black circles represent Ti-O column, big black circles represent Ba column, and white circles represent O column, respectively

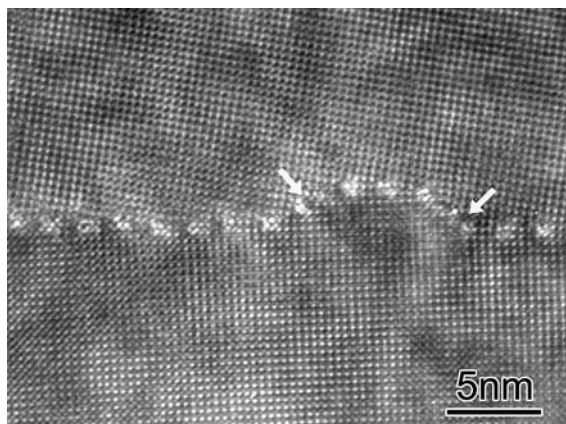
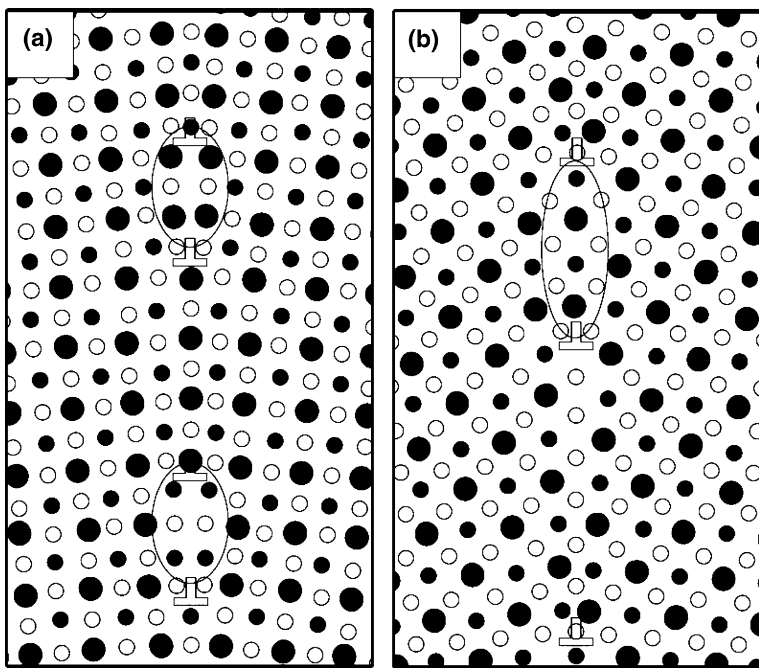


**Fig. 5** 12° [001] low-angle tilt boundary with (100) plane and (110) plane facet structure. The arrows indicate the dissociated two partials with the Burgers vector of  $\mathbf{b} = a/2[110]$ , where the boundary is composed of (110) plane

## Conclusion

Plan-view HRTEM observations were performed for [001] fiber-textured BaTiO<sub>3</sub> films fabricated by PLD. TEM observation revealed that low-angle tilt boundaries with the tilt angles below 15° are frequently (40%) found in the film.

The low-angle tilt boundaries were found to be classified into two types: boundaries with the boundary plane of (100) or (110). The (100) grain boundaries are composed of perfect type edge dislocations with the Burgers vector of  $\mathbf{b} = a[100]$ . The dislocations along

the (110) boundary planes, on the other hand, were dissociated into two partial dislocations with Burgers vectors of  $\mathbf{b} = a/2[110]$ . These stable dislocation structures should be related to the structure and energetics of the stacking faults on the boundary planes.

**Acknowledgements** This study was financially supported by the Japan Society for the Promotion of Science (JSPS).

## Reference

- Lewis GV, Catlow CRA, Casselton REW (1985) J Am Ceram Soc 68:555
- Heywang W (1971) J Mater Sci 6:1214
- Brandon DG, Ralph B, Ranganathan S, Wald MS (1964) Acta Metall 12:813
- Hayashi K, Yamamoto T, Ikuhara Y, Sakuma T (1999) J Appl Phys 86:2909
- Hayashi K, Yamamoto T, Ikuhara Y, Sakuma T (2000) J Am Ceram Soc 83:2684
- Oba F, Ohta H, Sato Y, Hosono H, Yamamoto T, Ikuhara Y (2004) Phys Rev B 70:125415
- Frank FC (1950) In: A symposium on the plastic deformation of crystalline solids. Office of Naval Research, Washington, DC, p 151
- Zhang Z, Sigle W, Kurtz W, Rühle M (2002) Phys Rev B 66:214112
- Lee B, Sigle W, Philipp F, Brunner D (2005) Acta Mater 53:1843
- Kung H, Hirth JP, Foltyn SR, Arendt PN, Jia QX, Maley MP (2001) Phisica C 357–360:959